

## Kyanite, andalusite, sillimanite, and related mineral assemblages in the Truchas Peaks region, New Mexico

JEFFREY A. GRAMBLING

Department of Geology, University of New Mexico  
Albuquerque, New Mexico 87131

### Abstract

The Truchas Peaks region of northern New Mexico includes an apparent equilibrium occurrence of the  $Al_2SiO_5$  triple point. Andalusite occurs in rocks at the southern end of the Truchas Peaks uplift. Kyanite is present along the eastern edge and sillimanite in the northern part. Kyanite, andalusite, and sillimanite coexist in the center of the area. Near the triple point zone, isograds are controlled by topography: kyanite occurs along ridges, kyanite-andalusite on hillsides and kyanite-andalusite-sillimanite in valleys. The distribution of minerals fits a model of near-horizontal isotherms and isobars, with pressures and temperatures increasing with depth and geothermal gradients increasing from north to south.

Where three aluminum silicates coexist, quartzite contains the assemblage chloritoid-staurolite-kyanite-andalusite-sillimanite-magnetite-hematite-quartz. Experimental data on the phase boundary  $Fe$  chloritoid +  $Al$  silicate =  $Fe$  staurolite + quartz at the hematite-magnetite  $f(O_2)$  buffer, corrected for minor elements, indicates temperature near  $535^\circ C$ . Garnet-biotite geothermometry gives a similar temperature. Pelitic schist contains cordierite-biotite-chlorite-kyanite-muscovite-quartz in the same area, and graphic and algebraic analysis suggests that this schist crystallized with  $X(H_2O)$  less than 1. Comparison with experimental data, taking into account mineral compositions and estimated  $X(H_2O)$ , yields  $T = 540^\circ C$ ,  $P(\text{total}) = 4$  kbar. Calculated  $P-T$  conditions are consistent with the position of the triple point according to Holdaway (1971).

### Introduction

The  $P-T$  conditions of invariant equilibrium in the  $Al_2SiO_5$  system are not well defined. Experimental determinations of the invariant point range from 2 to 8 kbar and 450 to  $850^\circ C$  (Zen, 1969; Richardson *et al.*, 1969; Brown and Fyfe, 1971; Holdaway, 1971). Several factors may be responsible for this experimental scatter, but all relate to the small free-energy differences among kyanite, andalusite and sillimanite close to equilibrium (Holdaway, 1971; Greenwood, 1976, p. 217-220).

Kyanite, andalusite and sillimanite coexist in the Truchas Peaks region of northern New Mexico. Geologic evidence indicates that they crystallized near equilibrium. The first part of this study documents this conclusion and interprets  $Al_2SiO_5$  isograd geometry in terms of regional variations in metamorphic pressures and temperatures.

The second part of this study addresses the  $P$  and  $T$  of the aluminum silicate invariant point. Chloritoid and staurolite coexist with kyanite, andalusite

and sillimanite in several rocks from the Truchas Range. Other rocks contain cordierite with chlorite, biotite, muscovite and  $Al$ -silicates. Because conditions for equilibrium among these minerals are known, they can be used to define the physical conditions at which the kyanite-andalusite-sillimanite assemblages formed.

### Geologic setting

The Truchas Peaks are located in the southern Sangre de Cristo Mountains, 35 km northeast of Santa Fe, New Mexico (see inset, Fig. 1). Metamorphic rocks are exposed in a  $5 \times 10$  km block-faulted uplift. Exposures are excellent, with topographic relief exceeding 1000 m and post-metamorphic faults providing structural relief in excess of several kilometers. Local relief is sufficient to allow three-dimensional mapping of isograds.

The Precambrian geology of the Truchas Peaks uplift is described by Grambling (1979b). Metamorphic rocks include massive crossbedded quartzite, pe-

litic schist and metavolcanic layers. These have been folded twice, isoclinally, with subparallel east-trending axes ( $F_1$  and  $F_2$ ) then gently refolded with northerly axes ( $F_3$ ). Prograde metamorphism overlapped the deformational events, but the present isograd geometry is post- $F_2$ . Metamorphism has not been dated in the Truchas Range. Similar rocks in nearby areas have yielded metamorphic ages near 1425 m.y. (Long, 1972; Gresens, 1975).

The Truchas Peaks lie 35 km southeast of the Picuris Range, New Mexico, another locality where kyanite, andalusite, and sillimanite coexist (Holdaway, 1978). The stratigraphic, structural, and metamorphic history of the Picuris Range is strikingly similar to that of the Truchas Range (Montgomery, in Miller *et al.*, 1963; Grambling, 1979b). The two mountain ranges are on opposite sides of the Picuris-Pecos fault, a structural feature which forms the western boundary of the Truchas Range, the eastern boundary of the Picuris Range and is at least 85 km long (Miller *et al.*, 1963). The two ranges may represent faulted parts of a single terrane, with the kyanite-andalusite-sillimanite assemblages of the Picuris Range being a westward continuation of the triple-point zone in the Truchas Range (Grambling, 1979b).

#### Techniques

Metamorphic rocks of the Truchas Range were mapped at a scale of 1:12,000. Electron microprobe analyses were performed on ARL-EMX microprobes at Princeton University and the University of New Mexico. Aluminum silicates were analyzed only for Fe, Al and Si because preliminary work detected no other elements. Other minerals were analyzed for the appropriate elements, using oxide and silicate standards. Reported analyses represent averages from 6 to 10 closely-spaced spots, with at least two grains of each mineral analyzed in each thin section. Microprobe data were reduced using a modified Bence-Albee (1968) scheme.

Accuracy of reported analyses is estimated at  $\pm 3\%$  of the amount present for oxides more abundant than 5 wt.%, and  $\pm 10\%$  for oxides less abundant than 1 wt.%. Al and Si have the largest relative errors. These estimates are based on multiple analyses of standards of known composition in the University of New Mexico collection.

#### Kyanite, andalusite, and sillimanite

Occurrences of kyanite, andalusite, and sillimanite are shown in Figure 1. Isograds denote the first ap-

pearance of andalusite or sillimanite and separate the map into four metamorphic zones. The kyanite zone contains only kyanite. The andalusite zone has andalusite  $\pm$  kyanite but no sillimanite. The sillimanite zone has sillimanite  $\pm$  kyanite but no andalusite. All three polymorphs coexist in outcrops along Rio Medio. This kyanite-andalusite-sillimanite zone occurs where the other three zones come together, suggesting that the triple-point rocks represent a close approach to equilibrium.

#### Kyanite-zone rocks

Kyanite occurs as 1 mm to 5 cm euhedral bladed crystals, as subhedral grains and as distinctly anhedral segregations. Most crystals are free of inclusions. Quartz and titanhematite (near  $\text{Hem}_{75}\text{Ilm}_{25}$ ) are the most abundant inclusions in those that are poikiloblastic. Kyanite typically defines planes of  $F_1$  foliation, suggesting that the mineral was present prior to first-generation folding. Some grains have been bent or granulated by  $F_2$  microfolds. However, kyanite shows textures indicating that it partially recrystallized after  $F_2$  deformation. Unstrained and randomly oriented crystals commonly occur as partial pseudomorphs after strained grains, and crystals that have overgrown  $F_2$  microfolds are not uncommon (Fig. 2).

#### Andalusite-zone rocks

Andalusite forms 2 to 10 cm poikiloblastic crystals (Fig. 3) that are riddled with quartz inclusions and commonly enclose small, ragged bits of kyanite, apparently relicts. Kyanite relicts are rimmed by 1 to 2 mm patches of non-poikiloblastic andalusite. Single andalusite crystals include many of these non-poikiloblastic patches linked together by wispy, dendritic stringers of andalusite. This type of texture may have resulted from nucleation of andalusite on a few of the pre-existing kyanite grains, followed by rapid replacement of surrounding kyanite.

Andalusite is rarely strained and many crystals have overgrown  $F_2$  microfolds. Kyanite relicts commonly are deformed. Textures are interpreted to mean that kyanite grew first, andalusite grew later, as rocks followed a  $P$ - $T$ -time path that crossed the kyanite-andalusite univariant boundary.

A few andalusite schists, from outcrops south of Pecos Baldy, contain no kyanite. Textural evidence suggests that andalusite in these rocks grew as a product of a reaction consuming chlorite + muscovite + staurolite, producing andalusite + biotite.

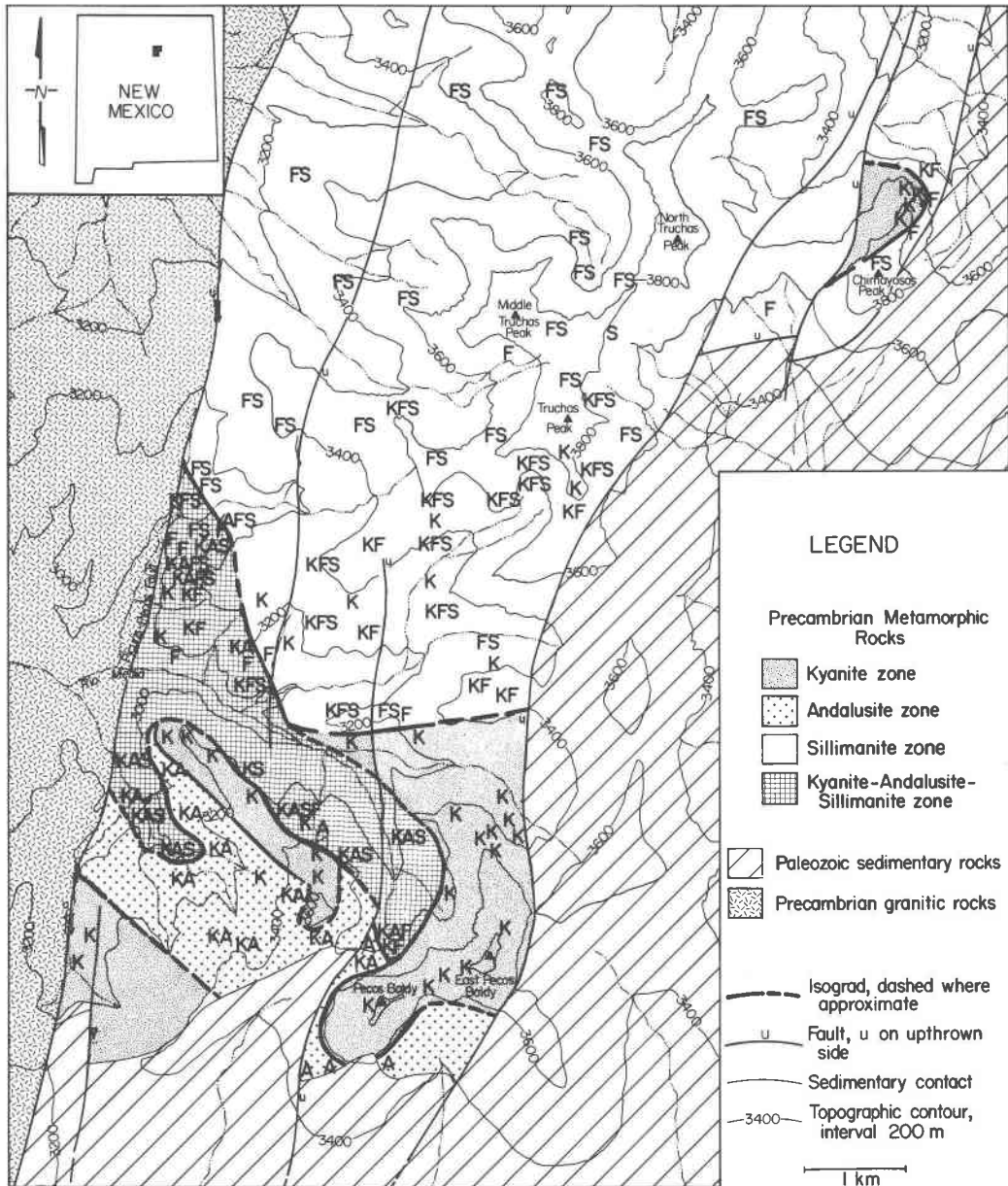


Fig. 1. Simplified geologic map of the Truchas Peaks region showing locations of samples containing kyanite (K), andalusite (A), coarse sillimanite (S), and fibrolitic sillimanite (F). Isograds denote first appearance of andalusite or sillimanite. Precambrian geology is shown in detail in Figure 6. Inset gives location.

### *Sillimanite-zone rocks*

Fibrolitic and coarse sillimanite occur throughout the sillimanite zone (Fig. 1). Fibrolite forms inclusion-free knots that are 1 to 20 mm in diameter. Some knots contain wormy, randomly oriented sillimanite fibers, but others show aligned bundles of fibrous sillimanite. Microprobe analyses of fibrolite show Si consistently in excess of 1.00 per 5 oxygens.

Mats of fibrolite are inhomogeneous with  $\text{SiO}_2$  ranging from 37 to 41 wt.%, a variation far greater than expected analytical error. Portions with high  $\text{SiO}_2$  show pale blue to white cathodoluminescence. Areas with stoichiometric Si, as well as coarse sillimanite, show no observable cathodoluminescence. These observations suggest that fibrolite is an intergrowth of extremely fine-grained sillimanite with quartz. A similar conclusion was reached by Bell and Nord

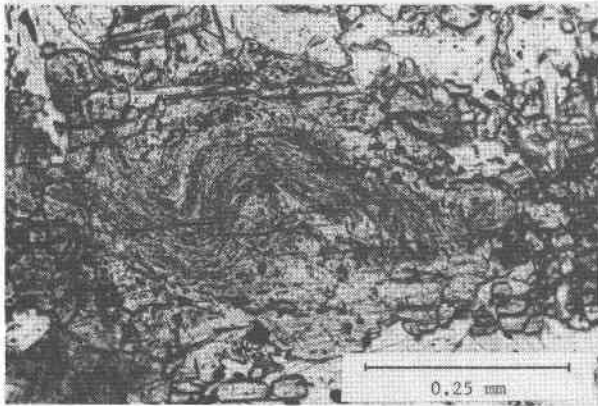


Fig. 2. Photomicrograph of kyanite that has overgrown  $F_2$  microfold. Fold is outlined by hematite-rich layers. Sample is from the north face of Pecos Baldy and contains kyanite + andalusite.

(1974) based on X-ray diffraction, electron diffraction and transmission electron microscopy.

Coarse sillimanite occurs as prismatic crystals up to  $5 \times 20$  mm. Where both varieties of sillimanite coexist, fibrolite appears to have coarsened into prismatic crystals. In several samples bundles of prismatic sillimanite form pseudomorphs after fibrolite. More typically sillimanite needles project outward from the edges of fibrolite knots (Fig. 4). Needles of sillimanite generally show a random orientation except in the northernmost, structurally deepest outcrops where they define a crude lineation.

Kyanite and sillimanite coexist at the southern end of the sillimanite zone. Kyanite persists up to 3 km north from the sillimanite isograd, but the mineral commonly has been embayed by fibrolite. Less commonly muscovite occurs in partial pseudomorphs after kyanite, with sillimanite developed nearby. These

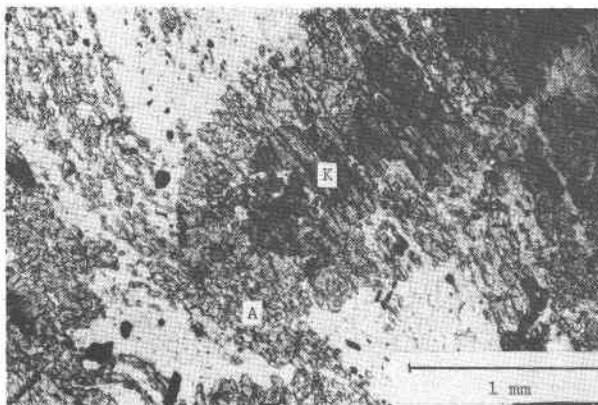


Fig. 3. Photomicrograph of poikiloblastic andalusite that includes corroded remnants of kyanite. Andalusite zone, north face of Pecos Baldy.

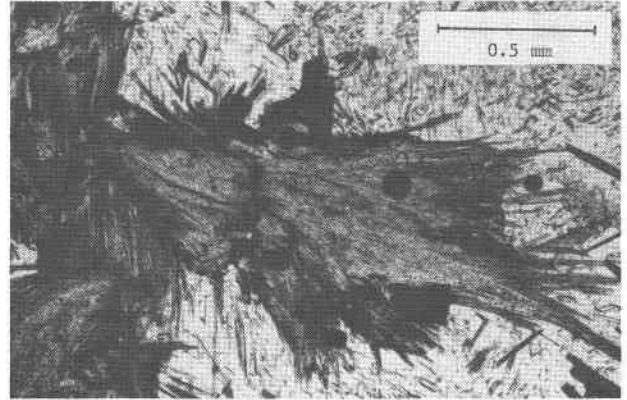


Fig. 4. Photomicrograph showing relationship between fibrolitic and coarse sillimanite. Sillimanite zone, from cirque south of Truchas Peak.

associations suggest that kyanite has inverted partially to sillimanite within the sillimanite zone, presumably when metamorphic conditions crossed the kyanite-sillimanite univariant boundary.

Holdaway (1971) suggested that the fine grain size of fibrolite might displace the reaction kyanite = fibrolite to a higher temperature than kyanite = sillimanite. Fibrolite and coarse sillimanite appear together at the kyanite-sillimanite isograd in the Truchas Range. The lack of a zone of coarse sillimanite, without fibrolite, adjacent to the isograd argues that the "fibrolite effect" which Holdaway encountered in experimental runs is not a problem in nature.

#### *Kyanite-andalusite-sillimanite-zone rocks*

Not all rocks within this zone contain kyanite + andalusite + sillimanite, but specimens containing each mineral can be found at most outcrops. Kyanite is the most common of the three at the eastern end of the zone. Sillimanite is most abundant at the northwestern end, and andalusite is most common within the prong that defines the southwestern corner of the triple-point zone.

The northwestern corner of the triple-point zone is defined as the portion north of Rio Medio but within 1 km of the Picuris-Pecos fault. Samples from this area show textures indicating a paragenetic sequence of kyanite  $\rightarrow$  andalusite  $\rightarrow$  sillimanite. Pseudomorphs of muscovite after kyanite are common. Fibrolitic to coarse sillimanite typically occurs as fringes around anhedral remnants of kyanite and andalusite. Kyanite and andalusite are interpreted to be relicts of pre-peak metamorphic conditions, with textures resulting from metamorphism along a  $P$ - $T$  path

that intersected the stability fields of kyanite and andalusite before peaking at a temperature slightly above the andalusite–sillimanite univariant boundary.

Andalusite clearly crystallized later than kyanite in the southwestern corner of the triple-point zone, but elsewhere the aluminum silicates tend to show no apparent order of crystallization (Fig. 5). In most rocks some kyanite grains have been deformed but others, together with andalusite and sillimanite, are unstrained. Most of the kyanite–andalusite–sillimanite zone apparently was metamorphosed to *P-T* conditions very near the equilibrium value for the  $Al_2SiO_5$  triple point.

Numerous quartz veins intrude quartzite and schist along the base of a 400 m deep cirque carved into the north face of Pecos Baldy, at the southeastern corner of the triple-point zone. These veins consist predominantly of milky white quartz. They are 5 to 30 cm across, up to 10 m long, and typically are lenticular. Sillimanite occurs as matted fibrolitic selvages, up to 5 cm thick, lining the quartz veins. Such sillimanite generally is associated with minor amounts of tourmaline and, in places, with kyanite and andalusite. Rocks more than 1 m away from such quartz veins contain kyanite and andalusite with only traces of sillimanite, suggesting that selvages are places where reactions that formed sillimanite proceeded to a greater extent than elsewhere in the rocks. Selvages may have formed from a type of contact metamorphism, induced by hot fluids migrating along channels now represented by quartz veins (Ferry, 1980, p. 380–381). These fluids may have been of metamorphic origin, migrating upward from deeper, hotter rocks. Alternatively, local con-

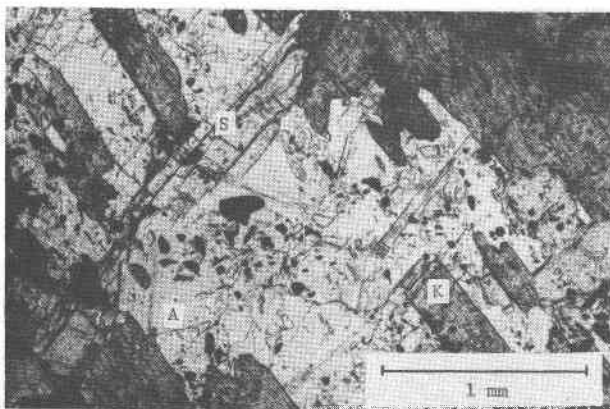


Fig. 5. Photomicrograph of specimen with kyanite (K), andalusite (A), and sillimanite (S) from triple point zone near Rio Medio.

Table 1. Microprobe analyses of kyanite, andalusite, and sillimanite

		76-	76-	76-	77-	77-	77-	77-
		472	529a	547	47	49	324	341a
		weight percent						
$Fe_2O_3^*$	Ky	.48	.89	.63	.46		.90	.59
	Andal				1.28	1.16	1.70	
	Sill	.56	.88	.59			.80	.71
$Al_2O_3$	Ky	63.11	62.09	63.25	63.51		61.60	62.66
	Andal				62.58	62.65	61.32	
	Sill	62.86	62.55	62.51			61.79	62.11
$SiO_2$	Ky	37.10	37.09	36.81	36.95		36.59	37.15
	Andal				36.86	36.79	36.41	
	Sill	36.92	37.36	37.08			36.39	37.11
Range in $Fe_2O_3$	Ky	.43-	.69-	.47-	.41-		.83-	.56-
	Andal	.53	1.09	.79	.51		1.41-	.63
	Sill				1.23-	1.14-	1.41-	
					1.33	1.21	1.96	
		.53-	.80-				.71-	.63-
		.58	.96				.99	.79
		cations based on 5 oxygens						
$Fe^{3+}$	Ky	.01	.02	.01	.01		.02	.01
	Andal				.03	.03	.04	
	Sill	.01	.02	.01			.02	.02
Al	Ky	2.00	1.98	2.00	2.01		1.99	1.99
	Andal				1.99	1.99	1.98	
	Sill	2.00	1.98	1.99			1.99	1.98
Si	Ky	1.00	1.00	.99	.99		1.00	1.00
	Andal				.99	.99	1.00	
	Sill	1.00	1.00	1.00			1.00	1.00
$K_e^{**}$		.999	1.001	1.001			1.002	.997
Oxides		HM	HM	HR	H	IR	HM	HR

\*All Fe as  $Fe^{3+}$

(Atoms Al, sill)/2

\*\* $K_e = \frac{(Atoms Al, ky)/2}{(Atoms Al, sill)/2}$ ; a - X models from Grew (1977)

and Halenius (1978)

H = hem M = mag I = ilm R = rutile

centrations of fluids may have acted as a simple catalyst in the polymorphic reactions.

#### Aluminum silicate chemistry

Most rocks that contain aluminum silicate minerals also contain primary hematite. The  $Fe^{3+}$  content of these aluminum silicates could be high (Strens, 1968; Albee and Chodos, 1969; Chinner *et al.*, 1969) and variable partitioning of  $Fe^{3+}$  might result in bivalent equilibrium between two polymorphs. Aluminum silicates were analyzed to test this possibility (Table 1).

Andalusite consistently has more Fe than kyanite and sillimanite which have similar  $Fe_2O_3$  contents. Single grains of all polymorphs show ranges in  $Fe_2O_3$  that are larger than would be expected from analytical error. Variations may reflect slight compositional inhomogeneities but probably result from varying degrees of contamination by microscopic hematite inclusions. Variations are all less than 0.3 weight percent  $Fe_2O_3$ , generally less than 0.1 weight percent, and do not affect the following discussion.

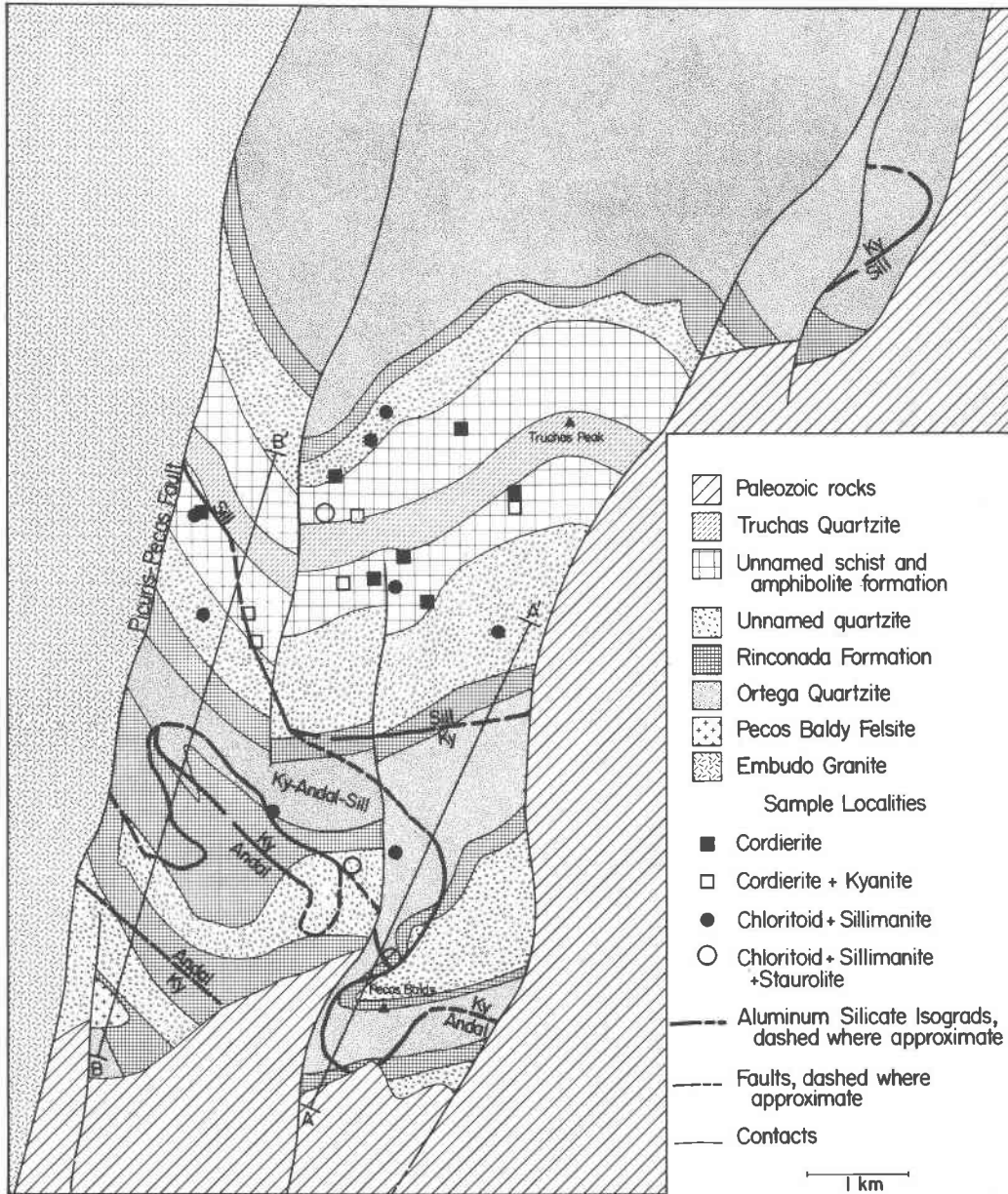


Fig. 6. Geologic map of the Truchas Peaks region showing mapped formations in Precambrian rocks. Aluminum silicate isograds, taken from Figure 1, and locations of chloritoid and cordierite-bearing samples are shown. Lines A-A' and B-B' refer to Figure 7.

Equilibrium constants ( $K_e$ ) have been calculated for coexisting kyanite and sillimanite using ideal ionic solution models (Table 1). If the zone of coexisting kyanite + sillimanite were due to bivariant equilibrium, then the two minerals should have different compositions and there should be spatial trends in Fe content and  $K_e$ . Three specimens (76-472, 76-529a and 76-547) were collected along a 3 km

traverse extending north from the kyanite-sillimanite isograd. Each is roughly an equal increment away from the isograd in the order listed. Inspection of Table 1 shows that there are no consistent trends in iron content or  $K_e$  among the three specimens, with  $K_e$  being virtually constant. This is inconsistent with bivariant equilibrium. Coexistence of kyanite + sillimanite is probably due to metastable persistence of

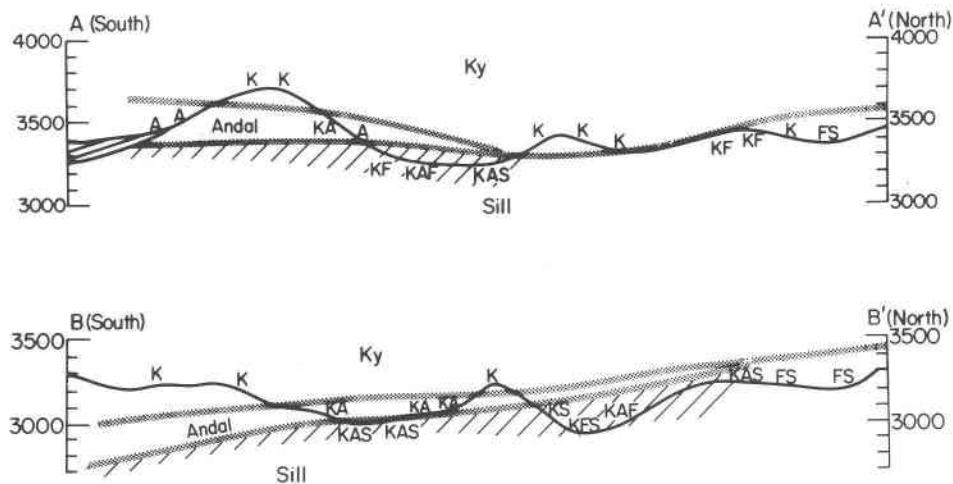


Fig. 7. Topographic cross-sections through the Truchas Range with aluminum silicate localities and isograds superimposed. Diagonal hachures represent areas where kyanite, andalusite, and sillimanite coexist. Section lines are from Figure 6. Vertical scale is elevation in m above sea level. No vertical exaggeration.

kyanite into the sillimanite stability field, an interpretation supported by Chinner *et al.* (1969) and Albee and Chodos (1969) in other areas.

#### *Geometry of aluminum silicate isograds*

Isograds cut across axial planes of first- and second-generation folds (Fig. 6), so the present isograd geometry must postdate  $F_2$  deformation. Third-generation structures are minor and have no apparent effect on isograd shapes.

However, there seems to be strong topographic control on Al-silicate zones. The topographically lowest part of the Truchas Range lies along Rio Medio and its tributaries. Rocks with kyanite, andalusite, and sillimanite occur only in the low area (Fig. 1). Samples collected from hillsides along the southern margin of the triple-point zone generally show andalusite  $\pm$  kyanite. Kyanite-zone rocks occur along ridge crests. Isograds have therefore been interpreted as subhorizontal surfaces.

Two north-south topographic cross sections appear in Figure 7. Section lines are shown in Figure 6. Aluminum silicate localities are plotted on the cross-sections and isograds, assumed nearly planar, are superimposed. The geometry of the resulting mineral zones is apparent. The kyanite zone overlies the andalusite zone which, in turn, overlies the sillimanite zone. The andalusite zone pinches out toward the north, allowing kyanite-zone rocks to rest directly above the sillimanite zone. Kyanite-andalusite-sillimanite assemblages occur in outcrops immediately below the andalusite-sillimanite isograd, implying that kyanite and andalusite persisted metastably

across much of the triple-point zone. Kyanite-andalusite-sillimanite rocks north of Pecos Baldy would appear to represent the closest approach to invariant equilibrium. However, assuming vertical geothermal gradients near  $40^\circ\text{C}/\text{km}$  during metamorphism, all rocks within the triple-point zone must have crystallized within  $20^\circ\text{C}$  and 150 bars of triple-point conditions. Kyanite-andalusite-sillimanite rocks disappear to the east because topography rises 400 m to the summits of Pecos Baldy and East Pecos Baldy, burying triple-point rocks beneath the kyanite zone.

Similar relationships between the kyanite and sillimanite zones can be seen near Chimayosos Peak in the northeastern corner of Figure 1. Kyanite-bearing rocks occur along the crest of a ridge running north from Chimayosos Peak. Outcrops at the base of a cliff, 100–300 m below the eastern edge of the ridge, contain fibrolitic sillimanite. Again, the sillimanite zone appears to be beneath the kyanite zone.

Two west-dipping reverse faults separate outcrops at Chimayosos Peak from the main part of the Truchas Range. Cumulative vertical offset across both faults, measured by displacement of formational contacts that dip south at  $60^\circ$ – $80^\circ$  (Fig. 6), is between 500 and 2000 m. If the kyanite-sillimanite isograd at Chimayosos Peak is projected westward across the faults, it would be 300–1800 m above the present summit of North Truchas Peak (3970 m). Since the isograd is exposed at 3353 m elevation 5 km south of the summit, the regional southward dip of the isograd is constrained to be between  $10^\circ$  and  $20^\circ$ . This agrees quite well with values shown on cross-sections in Figure 7.

Sections A–A' and B–B' (Fig. 7) are located on opposite sides of a rotational fault that strikes northerly, just west of Pecos Baldy (Fig. 6). The western side of that fault has been rotated, south-end-down, relative to the eastern side. This is seen best in dips of Paleozoic rocks: 25°S east of the fault and 35°S west of the fault. Aluminum silicate isograds also show this rotation. Isograds dip south at about 10° on the western side of the fault (B–B') but are horizontal on the eastern side (A–A'). Flexure in the kyanite–sillimanite isograd near the north end of section A–A' lies close to the hinge of rotation of the eastern fault block.

### Causes of isograd geometry

Although the arrangement of aluminum silicate zones seems to contradict standard beliefs that kyanite is the high-pressure polymorph, the geometry can be explained fairly simply. Rocks at the southern end of the Truchas Range show a paragenetic sequence kyanite → andalusite, indicating that they were metamorphosed along a *P–T* path that passed to the low-pressure side of the  $\text{Al}_2\text{SiO}_5$  triple point. Rocks from the northern end of the range show kyanite → sillimanite, indicating a *P–T* path to the high-pressure side of the triple point. The implication is that *P–T* conditions across the range bracketed the pressure and temperature of  $\text{Al}_2\text{SiO}_5$  invariant equilibrium.

A geothermal gradient of 40°C/km intersects the invariant point according to Holdaway (1971). Figure 8 shows isotherms and isobars plotted on a crustal cross-section for geotherms ranging from 36 to 45°C/km. Aluminum silicate isograds have been transferred onto the cross-section using experimental

data of Holdaway (1971). Any other experimental triple point would yield a similar isograd configuration.

Similarities between Figures 7 and 8 are obvious (see also Richardson, 1970, Fig. 7). Isograds in Figure 7 represent slight counterclockwise rotation of those in Figure 8. Counterclockwise (north-end-up) rotation of isograds is consistent with the southward dip of Paleozoic sedimentary beds, which presumably were horizontal when deposited, along the southern edge of the Truchas Range.

### Mineralogy of Fe silicates and oxides

Other minerals found in the Truchas Range are important in estimating the physical conditions of metamorphism.

Biotite is a solid solution of  $\text{KFe}_3\text{AlSi}_3\text{O}_{10}(\text{OH})_2$  to  $\text{KMg}_3\text{AlSi}_3\text{O}_{10}(\text{OH})_2$  with less than 0.5 wt.% MnO, 0.55 wt.% Na<sub>2</sub>O and 1.38 wt.% TiO<sub>2</sub> (Table 2). Microprobe data suggest minor substitutions of the type  $\text{Fe}^{\text{VI}} + \text{Si}^{\text{IV}} = 2 \text{Al}$  and also indicate that biotite is slightly deficient in alkalis.

Muscovite is principally a solid solution of  $\text{KAl}_3\text{Si}_3\text{O}_{10}(\text{OH})_2$  to  $\text{NaAl}_3\text{Si}_3\text{O}_{10}(\text{OH})_2$  to  $\text{KFeAlSi}_4\text{O}_{10}(\text{OH})_2$  to  $\text{KMgAlSi}_4\text{O}_{10}(\text{OH})_2$  with minor amounts of TiO<sub>2</sub> (Table 3). It typically shows a slight deficiency in alkalis. Muscovite contains up to 28 mol % paragonite in solid solution, but no primary paragonite occurs in any rocks of this study.

Chlorite forms a solid solution of  $\text{Fe}_5\text{Al}_2\text{Si}_3\text{O}_{10}(\text{OH})_8$  to  $\text{Mg}_5\text{Al}_2\text{Si}_3\text{O}_{10}(\text{OH})_8$  (Table 4). Most chlorites show excess Al and deficiencies in (Fe+Mg) and Si, suggesting the substitution  $\text{Fe}^{\text{VI}} + \text{Si}^{\text{IV}} = 2 \text{Al}$ . Chlorite also has minor amounts of TiO<sub>2</sub> and a maximum MnO content of 0.72 wt.%.

Chloritoid is a solid solution of  $\text{Fe}_2\text{Al}_4\text{Si}_2\text{O}_{10}(\text{OH})_4$  and  $\text{Mg}_2\text{Al}_4\text{Si}_2\text{O}_{10}(\text{OH})_4$  with minor amounts of MnO (up to 0.43 wt.%) and traces of ZnO and TiO<sub>2</sub> (Table 5). Microprobe data show 0.68 wt.% TiO<sub>2</sub> in chloritoid of sample 77-54a but these grains contain minute inclusions of rutile, suggesting that this high TiO<sub>2</sub> content is probably incorrect. Chloritoid systematically shows Fe + Mg + Mn + Zn in excess of 2.00 per 12 oxygens, coupled with slight deficiencies in Al. Because these rocks contain primary hematite, it is assumed that some of the Fe substitutes as  $\text{Fe}^{3+}$  for  $\text{Al}^{3+}$  in the mineral. Following Holdaway (1978), chloritoid that crystallized with hematite is assumed to have 9% of its iron as  $\text{Fe}^{3+}$ .

Cordierite is a solid solution of  $\text{Mg}_2\text{Al}_4\text{Si}_5\text{O}_{18}$  to  $\text{Fe}_2\text{Al}_4\text{Si}_5\text{O}_{18}$  with less than 0.8 wt.% MnO and traces of TiO<sub>2</sub> (Table 6). Cordierite shows  $\Delta = 0.28\text{--}0.30$

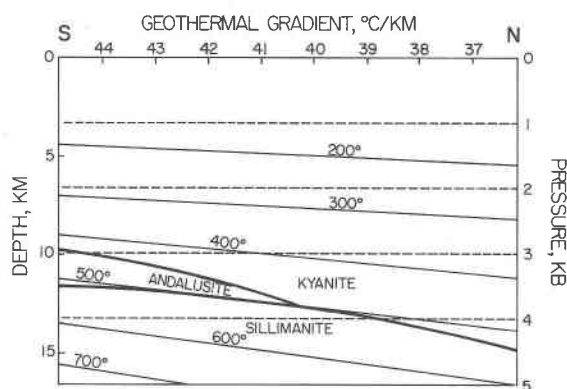


Fig. 8. Hypothetical cross-section of area where isobars (dashed) are at a slight angle to isotherms (light solid lines) during metamorphism. Corresponding geothermal gradients are shown at top of figure.  $\text{Al}_2\text{SiO}_5$  isograds have been superimposed using data of Holdaway (1971). Note similarity to Figure 7.

Table 2. Microprobe analyses of biotite

	76-492	76-531d	76-566	76-539a	77-74-f	77-199d	77-290a	77-292	77-324	77-338	77-341a	77-348a
weight percent												
FeO	15.80	15.62	9.90	11.72	13.20	9.97	11.20	11.16	13.05	10.82	11.47	10.55
MgO	13.72	13.66	18.91	15.46	15.68	15.60	14.96	15.42	14.35	17.20	15.23	16.01
MnO	.21	.36	.49	.18	.23	.15	.25	.27	.23	.44	.24	.33
TiO <sub>2</sub>	1.02	1.38	1.02	1.15	.79	.56	.94	1.14	.95	1.04	.98	1.15
Al <sub>2</sub> O <sub>3</sub>	20.05	20.05	19.66	18.49	19.02	18.13	19.73	19.65	19.92	19.74	19.43	19.60
SiO <sub>2</sub>	37.41	37.13	37.59	39.46	38.33	40.86	38.33	38.67	37.92	38.12	37.83	39.62
K <sub>2</sub> O	8.60	8.77	7.97	9.02	8.26	9.37	8.45	8.75	9.24	8.29	9.11	8.61
Na <sub>2</sub> O	.25	.22	.17	.26	.22	.40	.54	.26	.22	.46	.17	.40
Total	97.06	97.19	95.71	95.74	95.73	95.04	94.40	95.32	95.88	96.11	94.46	96.28
cations based on 11 oxygens												
Fe	.96	.95	.59	.71	.80	.60	.68	.67	.79	.65	.70	.63
Mg	1.49	1.48	2.02	1.66	1.70	1.67	1.63	1.66	1.56	1.84	1.66	1.70
Mn	.01	.02	.03	.01	.01	.01	.01	.02	.01	.03	.01	.02
Ti	.06	.08	.05	.06	.04	.03	.05	.06	.05	.06	.05	.06
Al	1.72	1.72	1.66	1.57	1.63	1.54	1.70	1.67	1.71	1.67	1.68	1.65
Si	2.72	2.70	2.69	2.85	2.78	2.94	2.80	2.80	2.76	2.73	2.77	2.82
K	.80	.81	.73	.83	.76	.86	.79	.81	.86	.76	.85	.78
Na	.04	.03	.02	.04	.03	.06	.08	.04	.03	.06	.02	.06
$\frac{Fe}{Fe + Mg}$	.39	.39	.23	.30	.32	.26	.29	.29	.34	.26	.30	.27
All Fe as FeO												

Table 3. Microprobe analyses of muscovite

	76-492	76-531d	76-566	77-199d	77-205	77-290a	77-292	77-324	77-338	77-341a	77-348a
weight percent											
FeO	2.63	2.68	2.57	1.86	1.46	3.02	2.49	3.13	3.04	2.83	2.67
MgO	.78	.59	.66	1.14	.67	.64	.61	.91	.89	.84	.86
TiO <sub>2</sub>	.49	.33	.16	.40	.21	.26	.31	.32	.46	.35	.09
Al <sub>2</sub> O <sub>3</sub>	36.25	36.97	36.71	36.45	37.19	35.22	36.20	35.40	35.38	35.13	35.63
SiO <sub>2</sub>	45.87	46.13	46.41	48.05	47.79	46.78	46.07	47.22	45.87	46.96	47.49
K <sub>2</sub> O	7.63	7.99	7.36	8.21	7.70	8.86	9.02	9.62	8.54	8.77	8.74
Na <sub>2</sub> O	1.14	1.56	1.89	1.85	1.65	1.18	1.31	.88	1.19	1.30	1.39
CaO	.00	.00	.00	.00	.00	.04	.00	.00	.00	.00	.00
Total	94.79	96.25	95.76	97.96	96.67	96.00	96.01	97.48	95.37	96.18	96.87
cations based on 11 oxygens											
Fe	.15	.15	.14	.10	.08	.16	.14	.17	.17	.16	.15
Mg	.08	.06	.06	.11	.06	.07	.06	.09	.09	.08	.08
Ti	.02	.02	.01	.02	.01	.02	.02	.02	.02	.02	.00
Al	2.83	2.86	2.84	2.76	2.83	2.74	2.82	2.72	2.77	2.73	2.74
Si	3.04	3.02	3.05	3.08	3.09	3.09	3.04	3.08	3.05	3.09	3.10
K	.65	.67	.62	.67	.63	.75	.76	.80	.72	.74	.73
Na	.15	.20	.24	.23	.21	.15	.17	.11	.15	.17	.18
Ca	.00	.00	.00	.00	.00	.01	.00	.00	.00	.00	.00
$\frac{K}{K + Na}$	.81	.77	.72	.74	.75	.83	.82	.88	.83	.81	.80

Table 4. Microprobe analyses of chlorite

	76-492	76-531d	76-539a	76-566	77-74f	77-199d <sup>1</sup>	77-205	77-290a <sup>1</sup>	77-292 <sup>1</sup>	77-338	77-341a	77-348a <sup>1</sup>
weight percent												
FeO	16.80	18.52	13.95	12.57	15.88	18.20	13.42	11.33	12.12	12.24	13.44	11.79
MgO	18.74	19.98	22.12	24.67	19.90	19.65	21.19	23.98	22.63	24.60	21.81	23.30
MnO	.66	.55	.30	.73	.48	.33	.14	.48	.45	.72	.63	.53
TiO <sub>2</sub>	.07	.10	.05	.35	.07	.10	.01	.08	.11	.03	.04	.07
Al <sub>2</sub> O <sub>3</sub>	22.64	22.84	23.20	24.35	23.57	23.32	23.55	23.49	23.53	24.09	23.76	24.41
SiO <sub>2</sub>	26.60	25.80	27.21	26.61	25.35	25.99	26.67	26.63	26.88	26.39	26.89	27.28
Total	85.51	87.79	86.83	89.28	85.25	87.59	85.88	85.97	85.72	88.07	86.57	87.38
cations based on 14 oxygens												
Fe	1.45	1.35	1.16	1.02	1.37	1.54	1.12	.94	1.02	1.00	1.12	.97
Mg	2.88	2.59	3.29	3.56	3.06	2.97	3.24	3.56	3.38	3.59	3.25	3.40
Mn	.06	.04	.03	.06	.04	.03	.01	.04	.04	.06	.05	.04
Ti	.01	.01	.00	.03	.01	.01	.00	.01	.01	.00	.00	.01
Al	2.75	2.34	2.73	2.78	2.86	2.79	2.79	2.76	2.78	2.78	2.80	2.82
Si	2.74	2.25	2.71	2.57	2.61	2.63	2.68	2.66	2.69	2.58	2.69	2.67
$\frac{Fe}{Fe + Mg}$	.33	.34	.26	.22	.31	.34	.26	.21	.23	.22	.26	.22

All Fe as FeO

<sup>1</sup>Retrograde chlorite

(Miyashiro, 1957) and has been assumed to include 0.5 moles H<sub>2</sub>O per 18 oxygens, after Bird and Fawcett (1974).

Garnet occurs in two samples and forms a solid so-

lution of almandine, pyrope, spessartine, grossular, and andradite (Table 6). Garnet in both samples has spessartine exceeding 25 mol %.

Staurolite is essentially a solid solution of

Table 5. Microprobe analyses of chloritoid

	76-391	77-53	77-54a	77-208	77-347a
weight percent					
FeO	28.67	26.11	28.82	28.43	28.03
MgO	.16	2.09	.01	.39	.03
MnO	.28	.43	.19	.39	.41
ZnO	.02	.04	.01	.00	.06
TiO <sub>2</sub>	.04	.02	.68	.02	.00
Al <sub>2</sub> O <sub>3</sub>	39.97	40.32	39.57	39.17	40.32
SiO <sub>2</sub>	23.77	24.10	24.14	23.86	23.90
Total	92.91	93.11	93.42	92.26	92.75
cations based on 12 oxygens					
Fe	2.02	1.81	2.01	2.01	1.97
Mg	.02	.26	.00	.05	.00
Mn	.02	.03	.01	.03	.03
Zn	.00	.00	.00	.00	.00
Ti	.00	.00	.04	.00	.00
Al	3.96	3.94	3.90	3.91	3.99
Si	2.00	2.00	2.02	2.02	2.01
$\frac{Fe}{Fe + Mg}$	.99	.88	1.00	.98	1.00

All Fe as FeO

Table 6. Microprobe analyses of cordierite and garnet

	76-539a cord	77-290a cord	77-292 cord	77-348a cord	76-539a gar	77-341a gar	
weight percent							
FeO	3.99	3.24	3.52	3.13	23.43	19.85	
MgO	10.37	11.24	10.89	10.88	4.27	4.49	
MnO	.48	.72	.75	.80	11.32	15.65	
CaO	.00	.00	.00	.00	2.74	1.66	
TiO <sub>2</sub>	.00	.01	.01	.01	.09	.02	
Al <sub>2</sub> O <sub>3</sub>	34.05	33.40	34.20	34.44	20.73	21.21	
SiO <sub>2</sub>	50.55	49.32	50.52	51.07	37.89	37.63	
Total	99.44	97.94	99.90	100.42	100.47	100.51	
cations based on 18 oxygens, cordierite; 12 oxygens, garnet							
Fe	.33	.28	.29	.26	1.56	1.32	
Mg	1.54	1.70	1.61	1.60	.51	.53	
Mn	.04	.06	.06	.07	.76	1.05	
Ca	.00	.00	.00	.00	.23	.14	
Ti	.00	.00	.00	.00	.01	.00	
Al	4.00	3.98	4.00	4.00	1.94	1.99	
Si	5.04	4.99	5.01	5.03	3.01	2.99	
$\frac{Fe}{Fe + Mg}$	.18	.14	.15	.14	.75	.71	
					Alm	.52	.44
					Spess	.25	.35
					Pyrope	.17	.18

All Fe as FeO

Table 7. Microprobe analyses of staurolite

	76-391	76-531d	77-53	77-54a	77-199d	77-205	77-208	77-290a	77-292	77-324	77-338	77-341a	77-347a
weight percent													
FeO	12.02	12.26	13.14	13.09	9.60	8.21	10.12	8.17	9.82	10.51	8.37	9.77	9.18
MgO	.20	2.20	.87	.13	1.21	1.21	.83	2.80	2.86	2.65	2.57	2.70	1.20
MnO	.42	1.05	.23	.23	.45	.19	.33	1.14	1.16	1.28	1.68	1.19	.95
ZnO	.49	1.05	.07	.17	1.88	1.50	4.34	3.29	2.51	2.10	3.93	3.08	4.84
TiO <sub>2</sub>	.37	.55	.50	.50	.49	.39	.22	.32	.47	.40	.37	.39	.38
Al <sub>2</sub> O <sub>3</sub>	56.21	52.55	55.63	56.33	55.44	57.22	54.50	54.43	55.12	53.26	53.20	53.45	53.98
SiO <sub>2</sub>	27.51	27.27	27.20	26.95	28.27	28.30	27.88	27.35	28.03	27.29	27.25	26.97	27.63
Total	97.22	96.93	97.64	97.40	97.34	97.02	98.22	97.50	99.97	97.49	97.37	97.55	98.16
cations based on 47 oxygens													
Fe	2.85	2.95	3.11	3.10	2.26	1.92	2.40	1.94	2.28	2.51	2.00	2.33	2.19
Mg	.08	.94	.37	.05	.51	.50	.35	1.18	1.18	1.13	1.10	1.15	.51
Mn	.10	.26	.06	.06	.11	.04	.08	.27	.27	.31	.41	.29	.23
Zn	.10	.22	.01	.04	.39	.31	.91	.69	.51	.44	.83	.65	1.02
Ti	.08	.12	.11	.11	.10	.08	.05	.07	.10	.09	.08	.08	.08
Al	18.76	17.81	18.56	18.83	18.40	18.84	18.23	18.18	18.01	17.91	17.94	18.00	18.11
Si	7.79	7.84	7.70	7.64	7.96	7.90	7.91	7.75	7.77	7.79	7.80	7.70	7.86
$\frac{Fe}{Fe+Mg}$	.97	.76	.89	.98	.82	.79	.87	.62	.66	.69	.65	.67	.81

All Fe as FeO

$Fe_4Al_{18}Si_8O_{48}H_2$  to  $Mg_4Al_{18}Si_8O_{48}H_2$ . Additional components include ZnO, .07 to 4.84 wt.%; MnO, .19 to 1.68 wt.%; and TiO<sub>2</sub>, .22 to .55 wt.% (Table 7). Analyses indicate a correlation between (Zn+Mn) and Fe/(Fe+Mg) in staurolite, with Fe/(Fe+Mg) decreasing as atomic (Zn+Mn) increases (Fig. 9), suggesting that Zn and Mn substitute for Fe rather than Mg in these staurolites (cf. Griffen and Ribbe, 1973). Staurolite also shows departures of R<sup>2+</sup>:Al:Si from the ideal formula (cf. Rumble, 1971).

Magnetite and rutile are pure Fe<sub>3</sub>O<sub>4</sub> and TiO<sub>2</sub>, respectively. Hematite ranges in composition from Hem<sub>65</sub>Ilm<sub>25</sub> to Hem<sub>85</sub>Ilm<sub>15</sub>, with traces of MnO (.02–.67 wt.%) and exsolved blebs of ilmenite. Primary ilmenite varies from Hem<sub>2</sub>Ilm<sub>98</sub> to Hem<sub>8</sub>Ilm<sub>92</sub> and has up to .09 wt.% MnO. No primary hematite–ilmenite pairs have been recognized, although magnetite in two ilmenite-bearing samples (77-53, 54a) is partly replaced by hematite which is pure Fe<sub>2</sub>O<sub>3</sub>, presumably a product of supergene alteration, and ilmenite in both samples is partly altered to an aggregate of hematite + rutile.

### Petrography

Chloritoid-bearing assemblages occur in 1–2 cm thick layers within massive quartzite. Chloritoid rarely occurs in pelitic beds, where common assemblages are staurolite–garnet–biotite–chlorite and staurolite–biotite–Al silicate–chlorite. Cordierite oc-

curs entirely within beds of hematitic schist and is limited to a single stratigraphic horizon that crops out in a band trending southwest from Truchas Peak. Cordierite schist, chloritoid quartzite, staurolite schist and chlorite–biotite–Al silicate quartzite are interlayered, with aluminum silicate minerals distributed throughout. Locations of chloritoid- and cordierite-bearing samples are superimposed on a geologic map in Figure 6.

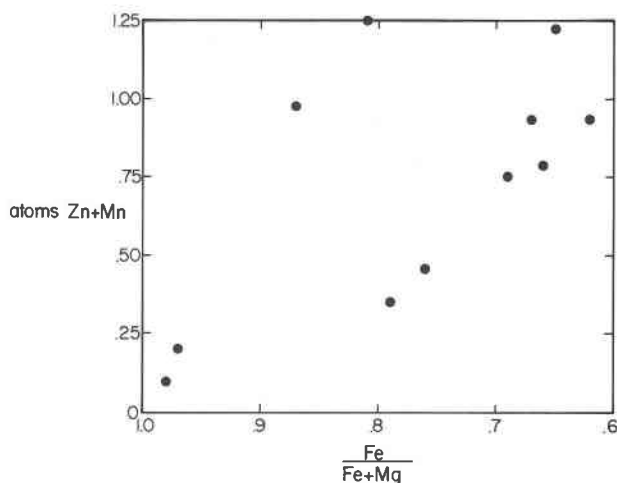


Fig. 9. Atomic Zn+Mn vs. Fe/(Fe+Mg) in staurolite. Apparent relationship can be expressed as  $(Zn+Mn) = -2.27 \frac{Fe}{Fe+Mg} + 2.44$  (linear regression,  $r^2 = 0.45$ ).

Table 8. Mineral assemblages in chloritoid quartzite

	Ctd	Stl	Ky	Andal	Sill	Mag	Rutile	Hem <sup>1</sup>
76-391	X	X	X	X	X	X		.70
76-392	X		X	X				X
76-469	X				X			X
77-53	X	X	X	X	X		X	.04
77-54a	X	X	X	X	X	X		.08
77-154	X	X						.65
77-165	X		X	X	X	X		X
77-199	X	X	X					X
77-208	X	X	X		X	X		.74
77-304	X		X		X		X	X
77-347a	X	X			X			.73
77-362	X		X		X		X	.68
77-363	X				X		X	.81
77-18	X					X		

<sup>1</sup>Numbers are X(Fe<sub>2</sub>O<sub>3</sub>) in hem or ilm; X means hematite present

All assemblages include quartz and muscovite

### Chloritoid quartzite

Chloritoid coexists with sillimanite in over 10 locations within the Truchas Range (Fig. 6). In three of these, chloritoid and sillimanite occur with staurolite. Two localities within the triple-point zone contain chloritoid-staurolite-kyanite-andalusite-sillimanite. Details of chloritoid-bearing assemblages are listed in Table 8.

All chloritoid quartzites contain 0.2–1.0 mm plates of hematite or ilmenite which are arranged parallel to foliation and are clearly primary. Primary ilmenite occurs only in samples 77-53 and 77-54a. Several specimens include blocky porphyroblasts of magnetite, and rutile occurs as isolated euhedra in sample 77-53. Excepting specimens 77-53 and 77-54a, no apparent supergene alteration has affected the FeTi oxides.

Table 9. Mineral assemblages in chlorite quartzite and schist

	Ch1	Al Sill	Biot	Stl <sup>2</sup>	Gar <sup>3</sup>	Plag	Hem <sup>1</sup>	Rut	Mag
76-492	X	S	X				.75	X	
76-531d	X	K,S	X	X		X	.73	X	
76-566	X	K,S	X	X	X		.75	X	
77-74f	X	K	X				X	X	
77-199d	X	K	X	X				X	
77-205	X	K,A		X			X		
77-241d	X	K,S	X	X	X	X	.70		
77-324	X	K,A,S	X	X			.75		X
77-338	X	K,S	X	X		X	.73	X	
77-341a	X	K,S	X	X	X	X	.71	X	

All samples include muscovite, quartz

<sup>1</sup> Numbers represent X(Fe<sub>2</sub>O<sub>3</sub>); X indicates hem present

<sup>2</sup> zincian staurolite

<sup>3</sup> manganese-rich garnet

Chloritoid is commonly in contact with Al silicate minerals. Staurolite, chloritoid, and aluminum silicates show no obvious replacement textures except in specimen 77-54a, where chloritoid and sillimanite are intergrown in several partial pseudomorphs after staurolite. There is consistent partitioning of major and trace elements between staurolite and chloritoid, suggesting that they crystallized in equilibrium. The presence of chloritoid + aluminum silicate in many samples, but of staurolite + chloritoid + aluminum silicate in a few, suggests that metamorphic conditions peaked near the temperature of staurolite-chloritoid-Al silicate-quartz equilibrium. The presence or absence of staurolite probably was controlled by minor factors such as local variations in  $f(\text{O}_2)$ ,  $f(\text{H}_2\text{O})$ , Zn, Ti or Fe/(Fe+Mg).

### Chlorite quartzite and schist

Mineral assemblages in chloritoid, cordierite-free quartzite and schist are shown in Table 9. Most have chlorite, muscovite, quartz, aluminum silicates and biotite; a few have zinc-rich staurolite, with ZnO greater than 1.5 wt.%; nearly all include hematite + rutile; and most have plagioclase, An<sub>7</sub> to An<sub>45</sub>.

Hematite occurs as plates aligned parallel to foliation and is interpreted as primary. Chlorite, forming 2–3 mm length-fast plates with normal interference colors, commonly is aligned parallel to foliation and is strained or kink-banded. The single exception is specimen 77-199d, where chlorite has grown as stubby grains replacing biotite. This chlorite is not strained; it cuts across foliation and includes needles of rutile presumably derived from breakdown of titaniferous biotite. Excepting 77-199d, chlorite is older than regional deformation. Metamorphic peak conditions are younger than regional deformation, hence chlorite must be prograde. Chemical data argue that chlorite and biotite crystallized in equilibrium: they show consistent partitioning of major and minor elements, and biotite is consistently higher in Fe/(Fe+Mg) than coexisting chlorite. Again, the exception occurs in specimen 77-199d, where chlorite has higher Fe/(Fe+Mg) than biotite.

Because all staurolite in this rock type is zincian, it is assumed that ZnO stabilizes staurolite. Likewise, garnet contains over 11 wt.% MnO and presumably is stabilized by manganese.

### Graphitic schist

Graphitic schist is exposed south and west of Pecos Baldy, within the andalusite zone but only several hundred meters from the triple point zone. Mineral

assemblages include garnet–biotite–chlorite, garnet–biotite–chlorite–staurolite, garnet–biotite–staurolite and biotite–staurolite–andalusite–chlorite, all with muscovite, quartz and graphite (Grambling, 1979 a,b). Garnet is nearly pure almandine–pyrope and biotite falls within the compositional range cited by Ferry and Spear (1978) as useful for garnet–biotite geothermometry. Garnet–biotite distribution coefficients ( $K_D$  Fe–Mg, gar–biot) average 0.14.

#### *Cordierite schist*

Cordierite, occurring in outcrops within the triple point zone and the sillimanite zone (Fig. 6), typically forms 2–5 cm anhedral crystals. In a few instances these consist of aggregates of smaller grains. Cordierite contains abundant inclusions, with quartz and FeTi oxides being the most common.

Table 10 shows mineral assemblages in cordierite schist. The majority include chlorite, biotite, plagioclase ( $An_{43-77}$ ), quartz, hematite, and rutile. Most have muscovite, and many show kyanite, andalusite or sillimanite. Zincian staurolite and spessartitic garnet occur in several cordierite-bearing rocks.

Kyanite generally is anhedral, in places engulfed by cordierite and elsewhere surrounded by biotite. However, kyanite has been observed in direct contact with all other minerals in most cordierite-bearing

rocks. Textural relationships suggest that kyanite may have been a reactant in a reaction producing cordierite + biotite, but the reaction may not have proceeded to completion.

Two generations of chlorite, biotite and muscovite growth can be documented in many cordierite rocks. Early chlorite, biotite, and muscovite, together with tabular FeTi oxides, define a penetrative foliation in the schist. Cordierite apparently grew after the regional deformation, because cordierite generally shows very little evidence of deformation. A second generation of chlorite, biotite, and muscovite is oriented randomly and partially replaces cordierite, kyanite, and early biotite, demonstrating that cordierite schist has undergone significant retrograde metamorphism. There are no differences in composition between primary and retrograde minerals in a given rock, so it appears that the phyllosilicates re-equilibrated their compositions during retrograde metamorphism. Chemical considerations (following section) support this observation.

#### **Analysis of equilibrium conditions**

##### *Graphic analysis*

FeTi oxide compositions are plotted on an FeO–TiO<sub>2</sub>–Fe<sub>2</sub>O<sub>3</sub> diagram in Figure 10. This plot ignores

Table 10. Mineral assemblages in cordierite schist

Sample	Cord	Chl	Bio	Musc	Ky	And	Sill	(Zn) Stl	(Mn) Gar	Plag	Mag	Rutile	Hem <sup>1</sup>
76-539A	X	X	X						X	X	X		.68
76-567	X	X	X						X	X			X
77-152C	X	X	X		X					X			X
77-290A	X	X	X	X	X	X		X		X		X	.79
77-292	X	X	X	X	X			X		X		X	.73
77-315	X	X	X							X		X	X
77-317	X	X	X		X				X	X	X		X
77-345	X	X	X	X								X	X
77-348A	X	X	X	X	X			X		X		X	.72
78-69	X	X	X							X		X	X
78-112	X	X	X	X			X			X			X

All assemblages include quartz

<sup>1</sup>Numbers represent X(Fe<sub>2</sub>O<sub>3</sub>) in hem; X means hem present

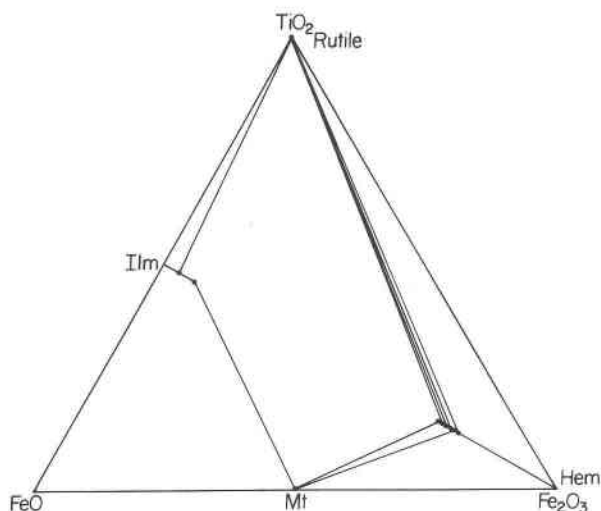


Fig. 10. FeTi oxide compositions and assemblages.

the trace amounts of MnO present in hematite (less than 0.7 wt.%) and ilmenite (less than 0.1 wt.%) but seems to work satisfactorily as a phase diagram. Lack of crossing tie lines is consistent with the hypothesis that the minerals represented attained chemical equilibrium. Application of the "method of equipotential lines" (Korzhinskii, 1959, p. 80–88) shows that  $\mu(\text{O}_2)$  decreases as mole fraction  $\text{FeTiO}_3$  in hematite increases in the assemblages hematite–rutile and hematite–magnetite.

The AFM projection (Thompson, 1957), however, shows a bewildering array of crossing tie lines and four-phase assemblages (Fig. 11). Crosscutting relations could be due to (1) retrograde effects; (2) failure

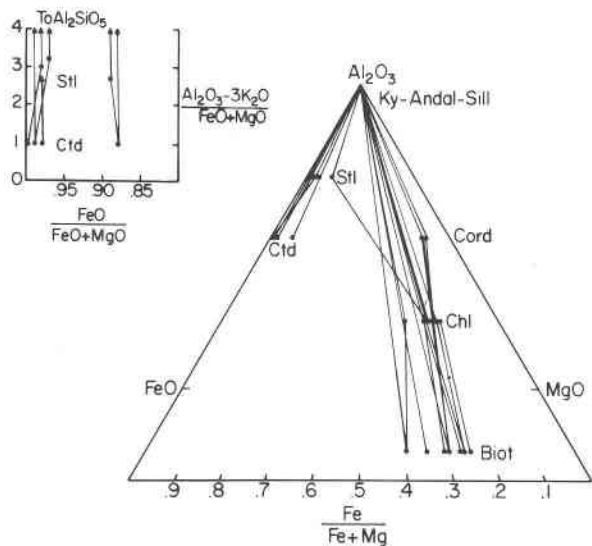


Fig. 11. AFM projection (Thompson, 1957) showing all rocks from the Truchas Range. See text for discussion of crossing tie lines. Inset is expansion of Al, Fe-rich portion of the projection.

of the projection to represent effects of minor components such as MnO, ZnO or  $\text{Fe}_2\text{O}_3$ ; or (3) failure of mineral assemblages to satisfy conditions under which AFM plots behave as phase diagrams (Rumble, 1978). The first explanation is not supported by mineral textures except in cordierite schist and specimen 77-199d, and removal of these rocks from the projection does not eliminate crossing tie lines. The second explanation removes one crossing tie line (staurolite–chlorite in 77-205), but other ties to zincian staurolite and spessartitic garnet are not shown in Figure 11. Other minerals have less than 0.8 wt.% MnO and 0.5 wt.% ZnO.

Differences in  $\text{Fe}_2\text{O}_3$  in the silicate minerals cannot be detected by electron microprobe but do not seem to cause crossing tie lines. AFM ties cross for assemblages that crystallized at equal  $f(\text{O}_2)$ , as indicated by equal  $X(\text{Fe}_2\text{O}_3)$  in hematite that coexists with rutile, and most assemblages have hematite + magnetite or hematite + rutile with nearly equal hematite compositions.

The AFM projection will resemble an equilibrium phase diagram only if all assemblages formed at the same  $P$ ,  $T$  and  $\mu(\text{H}_2\text{O})$ . Arguments presented earlier

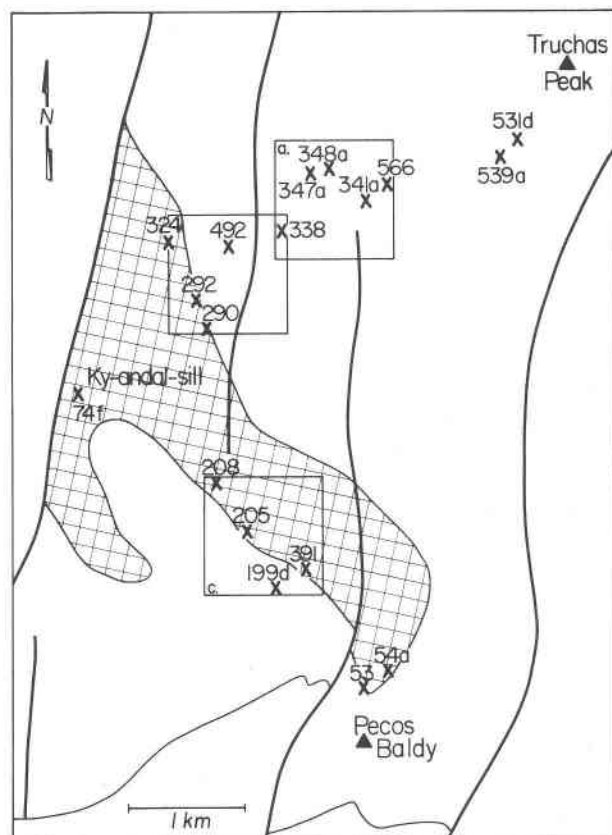


Fig. 12. Three 1 × 1 km areas discussed in text. Kyanite-andalusite-sillimanite zone is crosshatched.

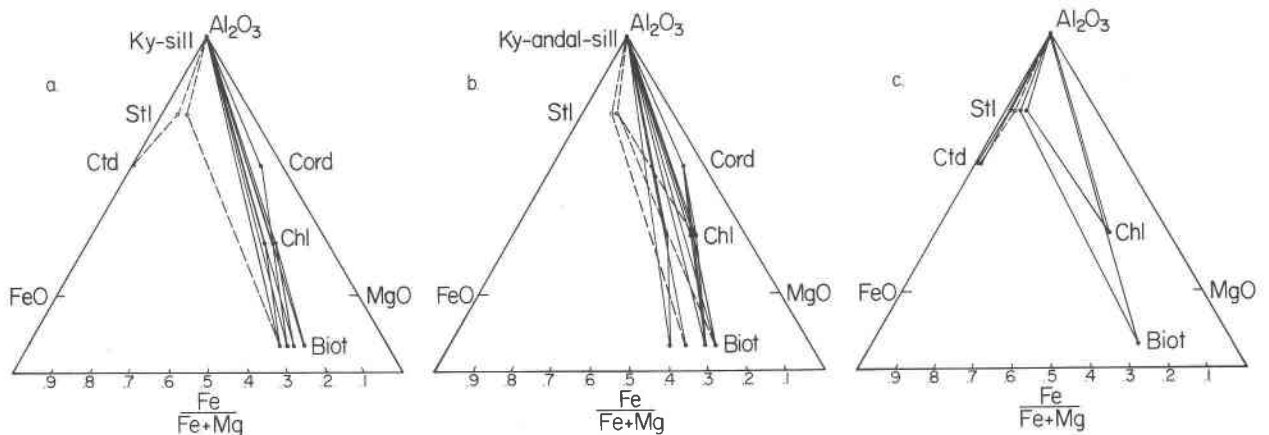


Fig. 13. AFM projections constructed for the three areas in Figure 12. Dashed tie lines are to zincian staurolites (Zn+Mn exceeds 2 wt.%) that do not plot strictly in AFM plane.

suggest that  $P$  and  $T$  were constant to  $\pm 150$  bars,  $\pm 20^\circ\text{C}$  across the triple point zone. However, a more convincing argument that variations in  $P$  or  $T$  did not cause the crossing tie lines is presented in Figures 12 and 13. Figure 12 shows three areas within the Truchas Range, each smaller than 1 km<sup>2</sup>, and Figure 13 shows AFM projections from the three areas. Tie lines cross in each projection. It seems reasonable to assume that  $P$  and  $T$  were constant within each small area, so variations in pressure or temperature apparently were not the cause of the crossing tie lines.

The possibility that rocks crystallized at variable  $\mu(\text{H}_2\text{O})$  can be evaluated by including  $\text{H}_2\text{O}$  in the projection plane. Nearly all the rocks contain muscovite, quartz, and an  $\text{Al}_2\text{SiO}_5$  mineral, so other minerals can be projected from these onto the plane  $\text{FeO}-\text{MgO}-\text{H}_2\text{O}$ . The resulting projection (Fig. 14) shows no crossing tie lines except in cordierite schist. Mineral textures described above indicate that cordierite schist has undergone retrograde metamorphism with partial recrystallization of chlorite, biotite, and muscovite. Presumably chlorite and biotite compositions were altered by this retrograde event so should not be plotted on phase diagrams with prograde minerals. Elimination of chlorite and biotite in cordierite schist removes all crossing tie lines from the plot.

The "method of equipotential lines" (Korzhinskii, 1959, p. 80-88) demonstrates that  $\mu(\text{H}_2\text{O})$  decreases as  $\text{Mg}/(\text{Mg}+\text{Fe})$  of chlorite and biotite increases in the assemblage chlorite-biotite-Al silicate-muscovite-quartz. The topology of Figure 14 requires that chlorite and biotite in equilibrium with cordierite, prior to retrograde metamorphism, must have had lower  $\text{Fe}/(\text{Fe}+\text{Mg})$  than chlorite and biotite in 76-566, the most Mg-rich chlorite and biotite shown.

Therefore,  $\mu(\text{H}_2\text{O})$  must have been lower in cordierite schist than in any cordierite-free chlorite schist.

Independent documentation of reduced  $X(\text{H}_2\text{O})$  in these rocks is provided by the presence of isolated  $\text{CO}_2$ -rich fluid inclusions in chlorite schist (Murck, Sisson and Hendel, Princeton University, preliminary work, personal communication, 1980).

#### Algebraic analysis

An estimate of the difference in  $\mu(\text{H}_2\text{O})$  between cordierite schist and chlorite schist can be made using the method of Rumble (1973, 1974, 1976, 1978),

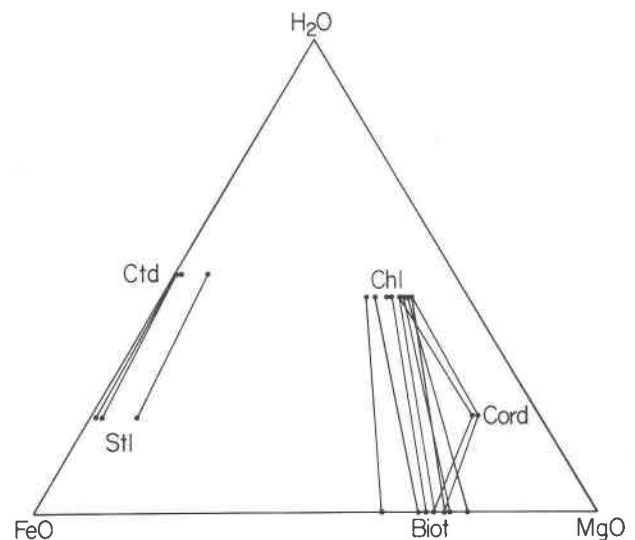


Fig. 14. Projection of minerals from quartz, muscovite, Al silicate onto plane  $\text{FeO}-\text{MgO}-\text{H}_2\text{O}$  using method of Greenwood (1975). All samples from Figure 11 are shown, but minerals with  $\text{ZnO} + \text{MnO}$  greater than 1 wt.% are omitted. Crossing tie lines are to retrograde chlorite and biotite in cordierite schist, see text for discussion.



Table 11. Ideal mineral formulas used in calculating equilibrium constants; abbreviations used in text and definition of symbols and components used in equation 2.

a. Ideal mineral formulas and abbreviations			
Kyanite	$Al_2SiO_5$	ky	
Andalusite	$Al_2SiO_5$	andal	
Sillimanite	$Al_2SiO_5$	sill	
Staurolite	$Fe_4Al_{18}Si_8O_{48}H_2$	stl	
Chloritoid	$Fe_2Al_4Si_2O_{10}(OH)_4$	ctd	
Chlorite	$Mg_5AlAlSi_3O_{10}(OH)_8$	chl	(c)
Cordierite	$Mg_2Al_4Si_6O_{10} \cdot 0.5H_2O$	cord	
Biotite	$KMg_3AlSi_3O_{10}(OH)_2$	biot	(b)
Muscovite	$KAl_2AlSi_3O_{10}(OH)_2$	musc	(m)
b. Components used in equation 2			
1. $Mg_{4.6}Al_{2.8}Si_{2.6}O_{10}(OH)_8$	2. $Fe_{4.6}Al_{2.8}Si_{2.6}O_{10}(OH)_8$		
3. $Mn_{4.6}Al_{2.8}Si_{2.6}O_{10}(OH)_8$	4. $Fe_{4.6}Al_{2.8}Ti_{2.6}O_{10}(OH)_8$		
5. $KMg_{2.7}Al_{1.6}Si_{2.7}O_{10}(OH)_2$	6. $KFe_{2.7}Al_{1.6}Si_{2.7}O_{10}(OH)_2$		
7. $KMn_{2.7}Al_{1.6}Si_{2.7}O_{10}(OH)_2$	8. $KFe_{2.7}Al_{1.6}Ti_{2.7}O_{10}(OH)_2$		
9. $NaMg_{2.7}Al_{1.6}Si_{2.7}O_{10}(OH)_2$			
10. $KAl_3Si_3O_{10}(OH)_2$	11. $KFeAlSi_4O_{10}(OH)_2$		
12. $KMgAlSi_4O_{10}(OH)_2$	13. $KAl_3Ti_3O_{10}(OH)_2$		
14. $NaAl_3Si_3O_{10}(OH)_2$			
15. $Al_2SiO_5$	16. $SiO_2$	17. $FeTiO_3$	
18. $Fe_2O_3$	19. $MnTiO_3$	20. $TiO_2$	
c. Other symbols used in equation 2			
$\bar{G}_{iJA}$	$= \frac{a^2 \bar{G}_i}{aX_{iA} aX_{jA}}$		
$X_{iA}$	= Mole fraction of i in mineral A		
A	$= \bar{G}_{11c} - \frac{\bar{G}_{14c}\bar{G}_{14c}}{\bar{G}_{44c}}$		
C	$= \bar{G}_{13c} - \frac{\bar{G}_{34c}\bar{G}_{14c}}{\bar{G}_{44c}}$		

tion 4 has been solved for chlorite schist specimens assuming metamorphic temperatures of 500°C and 600°C (Table 12). The equation also can be solved for cordierite schist by assuming a composition for equilibrium, pre-retrograde chlorite in cordierite schist. This is done in Table 12 using chlorite in 77-290a which is the most magnesium-rich chlorite in all the rocks,  $X_{1c} = .78$ . This is only 1% richer in  $X_{1c}$  than chlorite in 77-338, the most Mg-rich prograde chlorite, so calculations based on chlorite in 77-290a yield a maximum value for  $[\partial\mu(H_2O)/\partial X_{1c}]$  and for  $X(H_2O)$  in cordierite schist.

Estimates of the difference in  $\mu(H_2O)$  between any

Table 12. Values of  $\delta\mu(H_2O)/\delta X_{1c}$  for chlorite and cordierite rocks

Specimen	500°C	600°C
76-492	-5302 cal	-5988 cal
76-531d	-5302	-5988
76-566	-7610	-8594
77-74f	-5713	-6453
77-290a <sup>1</sup>	-8407	-9494
77-338	-8211	-9274
77-341a	-6978	-7881
average	-7037 cal	-8246 cal

<sup>1</sup>assemblage includes cordierite

two specimens may be obtained by taking the average value of equation 4 from table 12 and multiplying it by the difference in  $X_{1c}$  between the assemblages (Rumble, 1978). These are shown in Table 13.

Numerical estimates of differences in  $X(H_2O)$  among specimens can be derived from Table 13 using the expression for  $\mu(H_2O)$  in an ideal fluid (Rumble, 1978):

$$\mu(H_2O) = \mu^0(H_2O) + RT \ln X(H_2O)$$

These are presented in Table 14, relative to  $X(H_2O)$  in specimens 76-492 and 76-531d. Uncertainty associated with each value is  $\pm 10$  relative percent, based on  $\pm 3$  relative percent errors in microprobe analyses, provided the assumptions outlined above are valid.

If it is assumed that  $X(H_2O)$  in 76-492 and 76-531d was 1.0, then the values in Table 14 represent estimates of  $X(H_2O)$  in the different rocks during metamorphism. These estimates are *maximum* values, because it is possible that  $X(H_2O)$  was less than 1.0 in specimens 76-492 and 76-531d. The inferred  $X(H_2O)$  in cordierite schist, 0.56, is a maximum for a second

Table 13. Estimated differences in  $\mu(H_2O)$  in various samples relative to specimens 76-492 and 76-531d

Specimen	$\mu(H_2O), 492 - \mu(H_2O), \text{specimen; at } 500^\circ\text{C}$
76-492	0 cal
76-531d	0
76-566	-724
77-74f	-204
77-290a	-901
77-338	-838
77-341a	-577

Table 14. Estimated differences in  $X(\text{H}_2\text{O})$  relative to specimens 76-492 and 76-531d

Specimen	$X(\text{H}_2\text{O})$ relative to 76-492
76-492	1.00
76-531d	1.00
76-566	.62
77-74f	.88
77-290a <sup>1</sup>	.56
77-338	.58
77-341a	.69

<sup>1</sup>Assuming  $X_{1c, \text{chl}} = .78$

reason: equilibrium prograde chlorite in cordierite schist may have had higher  $X_{1c}$  than chlorite in specimen 290a. A minimum value for  $X(\text{H}_2\text{O})$  in cordierite schist can be established because  $\text{Mg}/(\text{Mg}+\text{Fe})$  of chlorite is lower than  $\text{Mg}/(\text{Mg}+\text{Fe})$  of coexisting cordierite (Ramsay, 1974; Guidotti *et al.*, 1975), and cordierite in these rocks has  $\text{Mg}/(\text{Mg}+\text{Fe}) = 0.85$ . This limits  $X(\text{H}_2\text{O})$  in cordierite schist to a minimum of 0.40, assuming  $X(\text{H}_2\text{O})$  in 76-492, 76-531d was 1.

### Physical conditions of metamorphism

Mineral assemblages in rocks of the Truchas Range include three independent geothermometers and one geobarometer that can be used to evaluate the pressure and temperature at which the kyanite-andalusite-sillimanite assemblages crystallized.

#### Garnet-biotite geothermometry

Garnet-biotite pairs in graphitic schist just south of the triple-point zone show  $K_D$  (Fe-Mg, gar-biot) = 0.14, corresponding to a temperature of  $505 \pm 50^\circ\text{C}$  (Ferry and Spear, 1978; A. B. Thompson, 1976). Graphitic schist lies entirely within the andalusite zone, so this temperature is a minimum for kyanite-andalusite-sillimanite assemblages.

#### Staurolite-chloritoid-Al silicate-quartz geothermometry

The assemblage staurolite-chloritoid-Al silicate-quartz is a useful geothermometer, provided attention is paid to  $f(\text{O}_2)$  and  $f(\text{H}_2\text{O})$ . This assemblage is relatively common in chloritoid quartzite within the triple-point zone where it coexists with hematite-magnetite, magnetite-ilmenite, and ilmenite-rutile (Table 8). Experimental investigations of the reaction



have been made by Richardson (1968) at the QFM  $f(\text{O}_2)$  buffer and by Ganguly (1972, 1977) at a range of  $f(\text{O}_2)$  values. Because most of the chloritoid-staurolite quartzites contain hematite or hematite + magnetite (Table 8), the experiments of Ganguly at the hematite-magnetite buffer are considered here. The experimental equilibrium temperature of reaction 5 lies in the range  $550\text{--}580^\circ\text{C}$  at the hematite-magnetite buffer and is not very sensitive to changes in total pressure.

Staurolite and chloritoid from chloritoid quartzite contain notable amounts of Mg, Mn, and Zn, so Ganguly's (1972, 1977) results are not directly applicable. However,  $P$ - $T$  conditions of the experimental curve can be corrected for solid solution effects using the van't Hoff approximation,

$$\ln K_i = - \frac{T^0 \Delta S_i^0}{R} \left( \frac{1}{T} - \frac{1}{T^0} \right) \quad (6)$$

if: (1) both staurolite and chloritoid behave as ideal ionic solutions, mixing on four and two sites, respectively; (2)  $\Delta C_p$  of the reaction is independent of temperature, in the temperature range considered; and (3) the entropy change of reaction can be estimated.

The equilibrium constant for reaction 5 is

$$K_5 = \frac{(X_{\text{FeStl}})^4 (X_{\text{H}_2\text{O}})^3}{(X_{\text{FeCtd}})^4}$$

given the assumptions above and considering ideal mixing in metamorphic fluid. Because of the strong effect of  $(\text{Zn}+\text{Mn})$  on  $\text{Fe}/(\text{Fe}+\text{Mg})$  in staurolite (Fig. 9), only staurolite with  $\text{Zn} + \text{Mn} < 1 \text{ wt.}\%$  has been used to calculate  $K_5$ . Chloritoid is assumed to have 9% of its Fe as  $\text{Fe}^{3+}$  and staurolite is assumed to have no  $\text{Fe}^{3+}$  (Albee, 1972, p. 3257). The corresponding value for  $K_5$  is 0.56 (*esd* .10), with  $X(\text{H}_2\text{O}) = 1$ .

All specimens of chloritoid schist did not crystallize at  $X(\text{H}_2\text{O}) = 1$ , as Figures 11 and 14 show. However, attempts to calculate differences in  $X(\text{H}_2\text{O})$  among the specimens are not useful because staurolite and chloritoid have similar values of  $\text{Fe}/(\text{Fe}+\text{Mg})$ , resulting in errors as large as  $\pm 50\%$  in calculated  $X(\text{H}_2\text{O})$  (Rumble, 1978). Therefore it is assumed that  $X(\text{H}_2\text{O})$  was near 1 in chloritoid schist. The entropy change of reaction 5 is estimated at  $2100 \text{ cm}^3\text{-bars/K mol}$  from Holdaway (1978). An error margin of  $\pm 50$  percent has been assumed.

The equilibrium temperature for reaction 5, calculated from equation 6 using  $K_5 = 0.56$ , is shown in Figure 15. It lies in the range  $530\text{--}540^\circ\text{C}$  for pres-

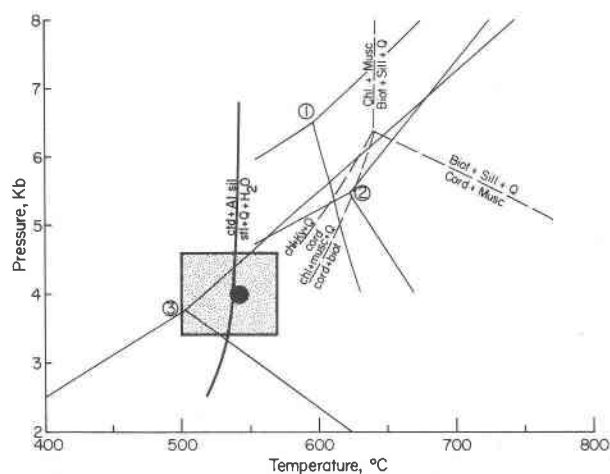


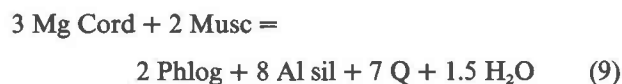
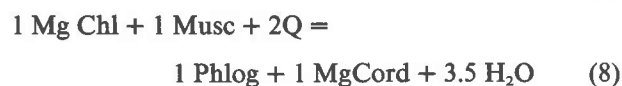
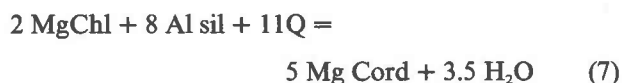
Fig. 15.  $P$ - $T$  conditions of metamorphism deduced from chloritoid quartzite (calculated equilibrium curve is plotted) and cordierite schist (heavy dot) in kyanite-andalusite-sillimanite zone. Uncertainty in  $P$ - $T$  conditions is indicated by stippled box. Shown for comparison are experimental kyanite-andalusite-sillimanite curves of Althaus (1967) labeled 1; of Richardson *et al.* (1969) labeled 2; and of Holdaway (1971) labeled 3. Dashed lines give experimentally determined positions of reaction 7-10 for  $X_{Mg} = 1$  and  $X(H_2O) = 1$  from Seifert (1970), Seifert and Schreyer (1970) and Bird and Fawcett (1973).

tures between 3 and 5 kbar. Effects of reduced  $P(H_2O)$  are not extreme: reduction of  $P(H_2O)$  to 0.6  $P$ (total) shifts the equilibrium curve to lower temperatures by only 25°C.

Error analysis indicates an uncertainty of  $\pm 30^\circ\text{C}$  (1 *esd*) in calculated equilibrium temperatures, including uncertainty in the experimental data.

#### Geothermometry and geobarometry based on cordierite schist

Mineral assemblages in cordierite schist can be used to define pressure and temperature of crystallization of the kyanite-andalusite-sillimanite rocks, since  $X(H_2O)$  in cordierite schist has been established above. Pertinent experimental data are shown in Figure 15, based on results of Seifert (1970), Seifert and Schreyer (1970), and Bird and Fawcett (1973). Balanced for an assumed cordierite water content of 0.5 moles, reactions are:



Reactions 7-10 intersect in an invariant point which, for the pure Mg system, lies close to 640°C and 6.5 kbar  $P(H_2O)$ . Variance of the assemblage increases as Fe, Mn, Ti, and Na are added.

Cordierite schist contains all phases present at the Mg invariant point (Table 10), if textural evidence for prograde chlorite and biotite is accepted. The  $P$ - $T$  conditions of the Mg invariant point can be corrected for solid solution effects and for reduced  $X(H_2O)$  by calculating the offset of any two of reactions 7-10, using equation 6, and determining their intersection graphically. Reactions 7 and 8 are best constrained by experimental results, so they were used in calculations. Estimates of  $\Delta S_7$  and  $\Delta S_8$ , obtained from experimental data and the Clausius-Clapeyron equation, are 6300 and 2500  $\text{cm}^3\text{-bars/K mol}$  respectively, based upon experimental results of Seifert and Schreyer (1970) and Seifert (1970). These have been assigned an uncertainty of  $\pm 50\%$ .

All minerals are treated as ideal ionic solutions, with biotite mixing on 3 sites, chlorite on 5, cordierite on 2 and muscovite on 1. Resulting equilibrium constants are:

$$K_7 = \frac{(X_{MgCord,Cord})^{10}(X_{H_2O})^{3.5}}{(X_{1c})^{10}}$$

$$K_8 = \frac{(X_{MgCord,Cord})^2(X_{Phlog,Biot})^3(X_{H_2O})^{3.5}}{(X_{1c})^5(X_{K,musc})}$$

Because the cordierite schist has undergone minor retrogradation, it is necessary to determine prograde, equilibrium mineral compositions to calculate  $K_7$  and  $K_8$ . For the calculation it was assumed that cordierite and muscovite have the correct compositions (Tables 3, 6) and that prograde chlorite and biotite had compositions equal to those in specimen 76-566, the most Mg-rich chlorite-biotite pair analyzed. Resulting equilibrium constants are  $K_7 = .77$  (*esd* .46),  $K_8 = .19$  (*esd* .09), for  $X(H_2O) = 0.56$  (*esd* .05).

Inserting these values for  $K_7$ ,  $K_8$ ,  $\Delta S_7$  and  $\Delta S_8$  into equation 6 and solving graphically yields a calculated pressure and temperature of 4 kbar and 540°C. Uncertainty in the calculation is  $\pm 600$  bars,  $\pm 25^\circ\text{C}$ . Additional uncertainty arises because (1) equilibrium compositions of chlorite and biotite are not well known; and (2) the value of  $X(H_2O) = 0.56$  is a maximum, as discussed above. Uncertainty associated with the first possibility is  $\pm 5^\circ\text{C}$  and  $\pm 100$  bars; that associated with the second would shift  $P$  and  $T$  to

lower values. Taking minimum  $X(\text{H}_2\text{O}) = 0.40$ , minimum values of  $P$  and  $T$  are 3650 bars and 505°C.

### Comparison to experimental data

The three independent geothermometers show remarkable agreement: 505±50°C for garnet–biotite, 535±35°C for chloritoid–staurolite, and 540±25°C for cordierite geothermometry. Cordierite geobarometry indicates a pressure of 4±0.6 kbar. Equilibrium conditions are shown graphically in Figure 15. Taken together, they imply that the kyanite–andalusite–sillimanite assemblages of the Truchas Peaks region crystallized near 535°C and 4000 bars total pressure. Reference to Figures 7 and 8 shows that these  $P$ – $T$  conditions must be slightly higher than those of true kyanite–andalusite–sillimanite equilibrium.

Figure 15 shows three experimental determinations of the  $\text{Al}_2\text{SiO}_5$  triple point. That of Althaus (1967) lies at pressures and temperatures considerably higher than those determined here. That of Richardson *et al.* (1969) lies at higher  $P$  and  $T$  also, although their region of uncertainty (Richardson *et al.*, 1969, Figure 2) nearly overlaps with the maximum  $P$  and  $T$  consistent with rocks from the Truchas Range. The determination of Holdaway (1971) is entirely consistent with data presented here. Kyanite, andalusite, and sillimanite from the Truchas Range have small and nearly equal  $\text{Fe}^{3+}$  contents (Table 1), so partitioning of  $\text{Fe}^{3+}$  among the Al silicates does not affect these comparisons.

### Conclusions

A suite of metasedimentary rocks in the Truchas Peaks area preserves what appears to be a near-equilibrium occurrence of the  $\text{Al}_2\text{SiO}_5$  invariant assemblage. This interpretation is supported by mineral textures, by the geometric distribution of mineral zones, and by a simple theoretical model that explains the distribution of mineral zones (Figs. 7, 8).

Graphical analysis of mineral equilibria has demonstrated that  $X(\text{H}_2\text{O})$  was less than unity in many of the metamorphic rocks. This has been substantiated by recognition of  $\text{CO}_2$ -rich fluid inclusions in chlorite schist (Murck, Sisson and Hendel, personal communication 1980). An isochor based on these fluid inclusions extrapolates through estimated  $P$ – $T$  conditions.

Algebraic analysis of equilibria has yielded numerical estimates of  $X(\text{H}_2\text{O})$  in rocks with the assemblage chlorite–biotite–Al silicate–muscovite–quartz–hematite–rutile. In cordierite schist  $X(\text{H}_2\text{O})$  was no higher

than 0.6 and may have been as low as 0.4. Other rocks also show reduced  $X(\text{H}_2\text{O})$ . Variations in  $X(\text{H}_2\text{O})$  in schist and quartzite occurred even though these rocks contain neither graphite nor carbonate. This suggests that extreme caution is necessary when applying experimental data for  $P(\text{H}_2\text{O}) = P(\text{total})$  to natural rocks.

The pressure–temperature conditions under which kyanite–andalusite–sillimanite assemblages formed have been deduced by several independent methods. Garnet–biotite geothermometry on andalusite-zone rocks within 500 m of the triple point zone yields  $T = 505\pm 50^\circ\text{C}$ . Chloritoid quartzite, containing the assemblage staurolite–chloritoid–kyanite–andalusite–sillimanite–quartz–magnetite–hematite, crystallized near 535°C. Mineral equilibria in cordierite schist indicate temperature near 540°C at 4±0.6 kbar total pressure. Apparently, the kyanite–andalusite–sillimanite assemblages crystallized near 535°C and 4 kbar total pressure.

These conditions must be slightly higher than those of the equilibrium  $\text{Al}_2\text{SiO}_5$  invariant point, because kyanite–andalusite–sillimanite assemblages occur slightly beneath (e.g., at slightly higher  $P$  and  $T$  than) the kyanite–andalusite and andalusite–sillimanite isograds (Fig. 7). The experimental triple point of Holdaway (1971), at 501°C and 3.76 kbar, seems to be directly applicable to these rocks.

### Acknowledgments

This project was begun in partial fulfillment of the requirements for the degree of Doctor of Philosophy in Princeton University. Financial support came from a variety of sources including a National Science Foundation fellowship, the New Mexico Bureau of Mines and Mineral Resources, the Department of Geological and Geophysical Sciences, Princeton University, the Department of Geology, University of New Mexico, National Science Foundation grant NSF-DES 75-03259/Hollister and Sandia National Laboratories.

Presentation of the data has benefitted greatly from comments by J. F. Callender, R. F. Fudali, M. J. Holdaway, L. S. Hollister, C. Klein and D. Rumble III. I extend special thanks to J. M. Ferry for a particularly helpful review.

### References

- Albee, A. L. (1972) Metamorphism of pelitic schists: reaction relations of chloritoid and staurolite. *Geological Society of America Bulletin*, 83, 3248–3268.
- Albee, A. L., and Chodos, A. A. (1969) Minor element content of coexistent  $\text{Al}_2\text{SiO}_5$  polymorphs. *American Journal of Science*, 267, 310–316.
- Althaus, E. (1967) The triple point andalusite–sillimanite–kyanite. An experimental and petrologic study. *Contributions to Mineralogy and Petrology*, 16, 29–44.
- Bell, P. M. and Nord, G. (1974) Microscopic and electron diffrac-

- tion study of fibrolitic sillimanite. Carnegie Institute of Washington Yearbook, 1973-1974, 444-448.
- Bence, A. E. and Albee, A. L. (1968) Empirical correction factors for the electron microanalysis of silicates and oxides. *Journal of Geology*, 76, 382-403.
- Bird, G. W., and Fawcett, J. J. (1973) Stability relations of Mg-chlorite-muscovite and quartz between 5 and 10 kb water pressure. *Journal of Petrology*, 14, 415-428.
- Brown, G. C., and Fyfe, W. S. (1971) Kyanite-andalusite equilibrium. *Contributions to Mineralogy and Petrology*, 33, 227-231.
- Burnham, C. W., Holloway, J. R., and Davis, N. F. (1969) Thermodynamic properties of water to 1000°C and 10,000 bars. Geological Society of America Special Paper, 132, 96 pp.
- Chinner, G. A., Smith, J. V., and Knowles, C. R. (1969) Transition-metal contents of  $Al_2SiO_5$  polymorphs. *American Journal of Science*, 267A, 96-113.
- Ferry, J. M. (1980) A case study of the amount and distribution of heat and fluid during metamorphism. *Contributions to Mineralogy and Petrology*, 71, 373-385.
- Ferry, J. M. and Spear, F. S. (1978) Experimental calibration of the partitioning of Fe and Mg between biotite and garnet. *Contributions to Mineralogy and Petrology*, 66, 113-117.
- Ganguly, J. (1972) Staurolite stability and related parageneses: theory, experiments and applications. *Journal of Petrology*, 13, 335-365.
- Ganguly, J. (1977) Compositional variables and chemical equilibrium in metamorphism. In *Energetics of Geological Processes*, ed. S. K. Saxena and S. Bhattacharji, p. 250-284. Springer-Verlag, New York.
- Grambling, J. A. (1979a) Isothermal prograde metamorphism and fluid diffusion, Truchas Peaks region, north-central New Mexico. *Geological Society of America Abstracts with Programs*, 11, 435.
- Grambling, J. A. (1979b) Precambrian geology of the Truchas Peaks region, north-central New Mexico, and some regional implications. *New Mexico Geological Society Guidebook*, 30th Field Conference, 135-143.
- Greenwood, H. J. (1976) Metamorphism at moderate temperatures and pressures. In *The Evolution of the Crystalline Rocks*, D. K. Bailey and R. Macdonald, eds., 187-260. Academic Press, London.
- Gresens, R. L. (1975) Geochronology of Precambrian metamorphic rocks, north-central New Mexico. *Geological Society of America Bulletin*, 87, 1444-1448.
- Grew, E. S. (1977) Petrologic implications of iron content of coexisting sillimanite and ilmenite. *Geological Society of America Abstracts with Programs*, 9, 996-997.
- Griffen, D. T. and Ribbe, P. H. (1973) The crystal chemistry of staurolite. *American Journal of Science*, 273A, 479-495.
- Guidotti, C. V., Cheney, J. T., and Conatore, P. D. (1975) Coexisting cordierite + biotite + chlorite from the Rumsford quadrangle, Maine. *Geology*, 3, 147-148.
- Halenius, U. (1978) A spectroscopic investigation of manganian andalusite. *Canadian Mineralogist*, 16, 567-576.
- Holdaway, M. J. (1971) Stability of andalusite and the aluminum silicate phase diagram. *American Journal of Science*, 271, 97-131.
- Holdaway, M. J. (1978) Significance of chloritoid-bearing rocks in the Picuris Range, New Mexico. *Geological Society of America Bulletin*, 89, 1404-1414.
- Korzhinskii, D. S. (1959) *Physicochemical Basis of the Analysis of the Paragenesis of Minerals*. Consultants Bureau, N.Y., 142 pp.
- Long, L. E. (1972) Rb-Sr chronology of Precambrian schist and pegmatite, La Madera Quadrangle, northern New Mexico. *Geological Society of America Bulletin*, 83, 3425-3432.
- Miller, J. P., Montgomery, A., and Sutherland, P. K. (1963) Geology of part of the southern Sangre de Cristo Mountains, New Mexico. *New Mexico Bureau of Mines and Mineral Resources Memoir* 11, 106 pp.
- Miyashiro, A. (1957) Cordierite-andalusite relations. *American Journal of Science*, 255, 43-62.
- Ramsay, C. R. (1974) The cordierite isograd in Archean metasediments near Yellowknife, N.W. T., Canada: variations on an experimentally established reaction. *Contributions to Mineralogy and Petrology*, 47, 27-40.
- Richardson, S. W. (1968) Staurolite stability in a part of the system Fe-Al-Si-O-H. *Journal of Petrology*, 9, 467-488.
- Richardson, S. W. (1970) The relation between a petrogenetic grid, facies series and the geothermal gradient in metamorphism. *Fortschritt Mineralogie*, 47, 65-76.
- Richardson, S. W., Gilbert, M. C., and Bell, P. M. (1969) Experimental determination of kyanite-andalusite and andalusite-sillimanite equilibria: the aluminum silicate triple point. *American Journal of Science*, 276, 259-272.
- Robie, R. A., Hemingway, B. S., and Fisher, J. R. (1978) Thermodynamic properties of minerals and related substances at 298.15 K and 1 Bar ( $10^5$  Pascals) pressure and at higher temperatures. *U. S. Geological Survey Bulletin* 1452, 456 p.
- Rumble, D. III (1971) Chloritoid-staurolite quartzites from the Moosilauke quadrangle, New Hampshire. *Carnegie Institute of Washington Yearbook*, 69, 290-294.
- Rumble, D. III (1973) Fe-Ti oxide minerals from regionally metamorphosed quartzites of western New Hampshire. *Contributions to Mineralogy and Petrology*, 42, 181-195.
- Rumble, D. III (1974) Gibbs phase rule and its application in geochemistry. *Journal of Washington Academy of Science*, 64, 199-208.
- Rumble, D. III (1976) The use of mineral solid solutions to measure chemical potential gradients in rocks. *American Mineralogist*, 61, 1167-1174.
- Rumble, D. III (1978) Mineralogy, petrology and oxygen isotopic geochemistry of the Clough Formation, Black Mountain, western New Hampshire, U.S.A. *Journal of Petrology*, 19, 317-340.
- Seifert, F. (1970) Low-temperature compatibility relations of cordierite in haplopetites of the system  $K_2O-MgO-Al_2O_3-SiO_2-H_2O$ . *Journal of Petrology*, 11, 73-99.
- Seifert, F., and Schreyer, W. (1970) Lower temperature stability limit of Mg cordierite in the range 1-7 kb water pressure: a redetermination. *Contributions to Mineralogy and Petrology*, 27, 225-238.
- Strens, R. G. J. (1968) Stability of  $Al_2SiO_5$  solid solutions. *Mineralogical Magazine*, 36, 839-849.
- Thompson, A. B. (1976) Mineral reactions in pelitic rocks: II. Calculations of some  $P-T-X$  (Fe-Mg) phase relations. *American Journal of Science*, 276, 424-454.
- Thompson, J. B. (1957) The graphical analysis of mineral assemblages in pelitic schists. *American Mineralogist*, 42, 842-858.
- Zen, E-an (1969) The stability relations of the polymorphs of aluminum silicate: a survey and some comments. *American Journal of Science*, 267, 297-309.